Bioconjugate Chemistry

Article

pubs.acs.org/bc

Gold Nanorods Carrying Paclitaxel for Photothermal-Chemotherapy of Cancer

Fei Ren,[†,#,Δ] Saheel Bhana,[†,Δ] Derek D. Norman,[†] Jermaine Johnson,[†] Lijing Xu,[‡] Daniel L. Baker,[†] Abby L. Parrill,[†] and Xiaohua Huang*[,†]

[†]Department of Chemistry and [‡]Bioinformatics Program, The University of Memphis, Memphis, Tennessee 38152, United States

Supporting Information

ABSTRACT: Nanotechnology-based photothermal therapy has emerged as a promising treatment for cancer during the past decade. However, heterogeneous laser heating and limited light penetration can lead to incomplete tumor cell eradication. Here, we developed a method to overcome these limitations by combining chemotherapy with photothermal therapy using paclitaxel-loaded gold nanorods. Paclitaxel was loaded to gold nanorods with high density (2.0×10^4 paclitaxel per gold nanorod) via nonspecific adsorption, followed by stabilization with poly(ethylene glycol) linked with 11-mercaptoundecanoic acid. Paclitaxel was entrapped in the hydrophobic pocket of the polymeric monolayer on the surface of gold nanorods, which allows direct cellular delivery of the hydrophobic drugs via the lipophilic plasma membrane. Highly efficient drug release was demonstrated in a cell membrane mimicking two-phase solution. Combined photothermal therapy and chemotherapy with the paclitaxel-loaded gold nanorods was shown to be highly effective in killing head and neck cancer cells and lung cancer cells, superior to photothermal therapy or chemotherapy alone due to a synergistic effect. The paclitaxel-gold nanorod enabled photothermal chemotherapy has the potential of preventing tumor reoccurrence and metastasis and may have an important impact on the treatment of head and neck cancer and other malignancies in the clinic.

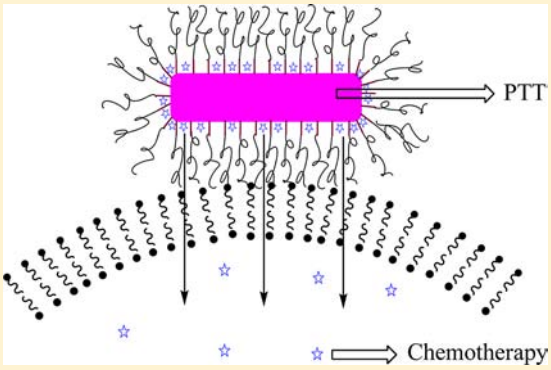

INTRODUCTION

During the past decade, nanotechnology-enabled photothermal therapy (PTT) has emerged as a potential anticancer treatment and generated a great deal of interest in nanomedicine. This technique is based on the use of nanostructures, including silica/gold nanoshells,[1−5] gold nanorods (Au NRs),[6−10] gold nanocages and hollow gold nanospheres,[11−14] and carbon nanotubes[15] that absorb light strongly within the tissue-transparent near-infrared (NIR) region. Treatment with nanoparticles (NPs) and subsequent irradiation with an NIR laser creates heat sufficient to induce tumor ablation. In comparison to other approaches, nanotechnology-based PTT has several advantages. It is a noninvasive and localized treatment. The anticancer effect is instant and the degree of effect can be controlled by the applied dosage of the external light. The therapeutic effect does not require intracellular uptake of the nanodrugs. However, PTT faces significant barriers. Complete eradication of cancer cells under laser irradiation is difficult because of the uneven heat distribution within the tumor caused by the heterogeneous distribution of NPs and the Gaussian distribution of the energy of the laser beam. In addition, the applied light intensity gradually reduces as it travels through tissue, leading to inefficient killing of tumor cells in deeper tissues. Thus, new strategies are needed to overcome these limitations.

One of the most promising approaches is to combine PTT with chemotherapy. Combined PTT and chemotherapy has been shown to be more effective than the two treatments alone due to additive or synergistic effects.[16−25] For example, Chan and co-workers reported that the combination therapy with Au NR-enabled hyperthermia and physically mixed cisplatin led to 84% more cell killing than hyperthermia alone and 78% more than cisplatin alone.[16] Combination therapy is also capable of reducing chemotherapy-associated toxicity by means of lowering the effective drug dosage. However, current methods depend mainly on a light-triggered mechanism to release the chemotherapeutic drugs from the nanocarriers.[18−25] Such treatments can be finely controlled through manipulation of the externally applied laser light. This approach prevents systemic toxicity due to off-target release of chemotherapeutic drugs. However, tumor cells in deep tissues may not be destroyed due to limited laser penetration.

Here, we report a new system for combined PTT and chemotherapy using NIR-absorbing Au NRs carrying chemotherapeutic paclitaxel (PTX). We made highly integrated PTX-Au NR complex in which PTX was entrapped with high density in the hydrophobic pocket of alkanethiol-linked poly(ethylene

Received: August 13, 2012
Revised: January 9, 2013
Published: January 29, 2013

   dx.doi.org/10.1021/bc300442d | *Bioconjugate Chem.* 2013, 24, 376−386

Scheme 1. Schematic Illustration of the Synthesis of MUA-PEG/PTX/Au NRs[a]

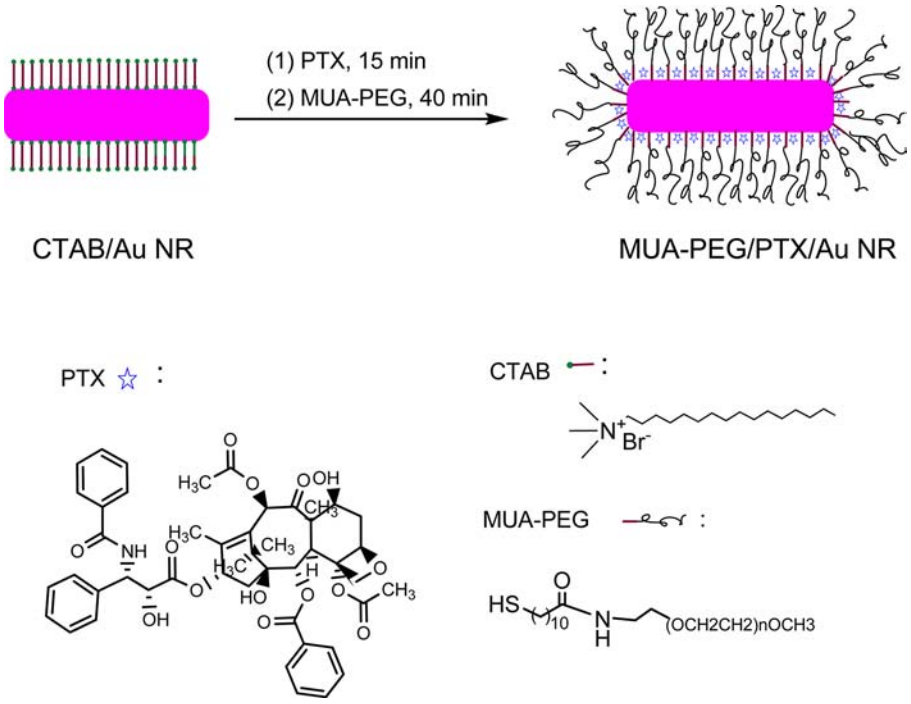

[a]MUA-PEG/PTX/Au NRs were formed by nonspecific adsorption of PTX onto Au NRs followed by stabilization with MUA-PEG. The molecular weight of PEG is 5000.

glycol) (PEG) monolayer on the surface of Au NRs. The nanocomplex allows drug release and cellular delivery of the hydrophobic drug through partitioning of the drug within the lipophilic plasma membrane, which is light-independent. The chemotherapeutic drug can therefore eradicate malignant cells outside the laser path, overcoming the limitation associated with PTT. We demonstrated that the PTX-Au NR complexes did not exhibit significant drug release in cell-absent environments, but efficiently released their payload in a cell-membrane-mimicking two-phase solution. The combined PTT and chemotherapy with the PTX-Au NR complex showed excellent efficacy for the treatment of cancer cells of different origin, superior to PTT or chemotherapy alone. As the nanocomplex uses a hydrophilic PEG protective layer that minimizes nonspecific uptake by the reticulo-endothelial system (RES),[26] passive tumor targeting would be achieved for in vivo and clinic applications through the enhanced permeability and retention (EPR) effect of solid tumors.[27] The novel single-particle drug delivery system may have an important impact on preventing cancer reoccurrence and metastasis.

EXPERIMENTAL PROCEDURES

Materials. All chemicals were purchased from Sigma-Aldrich unless specified. Amine-terminated poly(ethylene glycol) (PEG-NH_2, MW 5000) was purchased from Laysan Bio (Arab, AL). PTX was purchased from LC Laboratory (Woburn, MA).

Synthesis and Characterization of Au NRs. Au NRs with an aspect ratio of 3.7 were synthesized according to the seed-mediated growth method.[28] Briefly, 2 to 5 nm Au NPs were synthesized as a seed solution by the reduction of chloroauric acid ($HAuCl_4$) (2 mL, 0.25 mM) with ice-cold sodium borohydride ($NaBH_4$) (120 μL, 10 mM) in the presence of 0.1 M CTAB. A growth solution (100 mL) containing 0.5 mM $HAuCl_4$, 0.1 M CTAB, and 80 uM $AgNO_3$ was prepared, followed by the addition of ascorbic acid (1.40 mL, 80 mM). A volume of 140 μL of the seed solution was injected into the growth solution, followed by 10 s of mixing and 2 h of standing to allow completion of NR growth. The resulting Au NRs were purified via three rounds of centrifugation and wash (12 000 rpm, 20 min, Eppendorf 5804 R) and were stored in ultrapure water at RT. Optical absorption spectrum was measured using a UV−vis-NIR absorption spectrometer (Agilent, Santa Clara, CA). The NRs were quantified using the extinction coefficient determined by Orendorff et al.[29] The morphology and size of the NRs were determined using transmission electron microscopy (TEM) (Joel JEM1200 EX II, Tokyo, Japan). Hydrodynamic size and zeta potential were measured by dynamic light scattering (DLS) (Brookhaven 90 plus particle size analyzer, Holtsville, NY).

Synthesis and Characterization of 11-Mercaptoundecanoic Acid-Linked Poly(ethylene glycol) (MUA-PEG). MUA (final concentration: 1 mM) was dissolved in 4 mL of anhydrous dichloromethane (DCM), followed by the addition of PEG-NH_2 (10 mg) and 4-(dimethylamino) pyridine (DMAP) (0.1 mg). Then, *N,N′*-dicyclohexylcarbodiimide (DCC) (0.8 mg) was added and the mixture was stirred overnight in the dark. After solvent evaporation, the residue was reconstituted with ultrapure water and was purified with a 0.2 um filter to separate excess organic precipitates. Then, dithiothreitol (DTT) (final concentration: 1 mM) was added and the solution was stirred for 30 min in the dark. The final solution was purified by three cycles of centrifugation (8500 rpm, 20 min) using a centrifugal filter (MWCO 3000, Millipore). The product was characterized by absorption spectroscopy and nuclear magnetic resonance (NMR) spectroscopy. To collect the NMR spectrum, the sample was

dx.doi.org/10.1021/bc300442d | *Bioconjugate Chem.* 2013, 24, 376−386

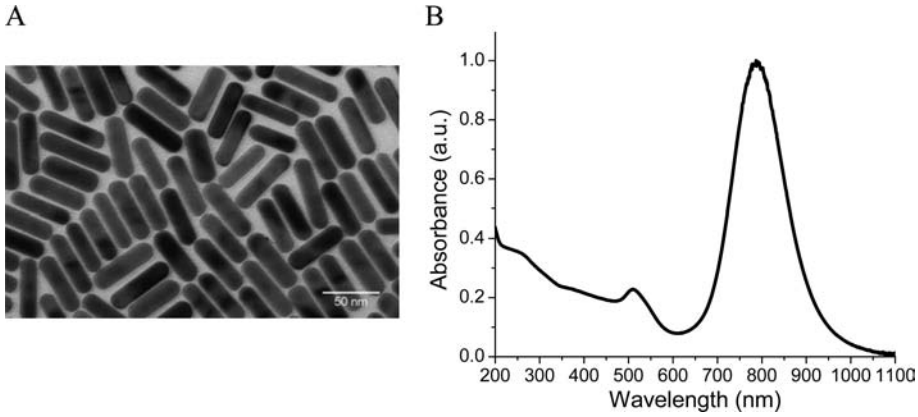

Figure 1. (A) TEM micrograph and (B) absorption spectrum of Au NRs. Au NRs had an aspect ratio of 3.7, with the surface plasmon resonance peaks at 520 and 780 nm.

lyophilized in the dark overnight, followed by reconstitution with deuterated chloroform ($CDCl_3$). ^1H spectrum was recorded on a Varian 500 MHz NMR spectrometer. ^1H spectra of MUA and NH_2−PEG were collected for comparison. ^1H NMR ($CDCl_3$) for MUA: δ 1.29 (m, 12H), 1.34 (t, 1H, J = 7.6 Hz), 1.62 (m, 4H), 2.36 (t, 2H, J = 7.6 Hz), 2.53 (q, 2H, J = 7.6 Hz), 11.25 (br s, 1H); ^1H NMR ($CDCl_3$) for NH_2−PEG: δ 1.80 (br s, 2H), 2.92 (t, 2H, J = 5.2 Hz), 3.38 (s, 3H), 3.52 (m, 2H), 3.54−3.83 (m, 418 H); ^1H NMR ($CDCl_3$) for MUA-PEG: δ 1.28 (m, 12H), 1.34 (t, 1H, J = 7.3 Hz), 1.62 (m, 4H), 1.83 (m, 14H), 2.17 (t, 2H, J = 7.3 Hz), 2.41 (t, 1H, J = 7.3 Hz), 2.53 (q, 2H, J = 7.6 Hz), 2.67 (t, 1H, J = 7.3 Hz), 2.85 (t, 2H, J = 7.3 Hz), 3.38 (s, 3H), 3.53 (m, 2H), 3.58−4.20 (m, 423H), 5.35 (br s, 1H), 6.24 (s, 1H).

Preparation and Characterization of PTX-Loaded, MUA-PEG-Stabilized Au NRs (MUA-PEG/PTX/Au NRs). PTX dissolved in dimethyl sulfoxide (DMSO) (6 uL, 5 mM) was added to Au NRs (1 mL, 0.5 nM) and the mixture was stirred for 15 min (Scheme 1). Then, MUA-PEG (30 uL, 1 mM) was added and the solution was stirred for 40 min. The MUA-PEG/PTX/Au NRs were purified by three rounds of centrifugation (12 000 rpm, 20 min) and the residue was reconstituted with ultrapure water. The nanocomplexes were characterized by absorption spectroscopy and DLS. To determine PTX content, the nanocomplexes (100 uL, 0.5 nM) were mixed with DCM (500 uL) with vigorous stirring. After 4 h, the DCM solution was collected and the solvent was removed by evaporation. The residue was reconstituted with methanol and analyzed on an Acquity UPLC system coupled with mass spectrometry (Waters, Milford, MA) with a reverse-phase C_{18} column (pore size: 1.7 um). The number of MUA-PEG was determined using the *N*-succinimidyl 3-(2-pyridyldithio) propionate (SPDP) method.[30] In this method, we assumed thiolated PEG with the same molecular weight have similar binding affinity to Au NRs. Thus, the number of MUA-PEG on Au NRs was determined using HS-PEG-NH_2. The number of HS-PEG-NH_2 on Au NR was determined by the reaction of SPDP with the primary amine to generate pyridine-2-thione that can be quantified by UV−vis absorption.[31]

Stability of MUA-PEG/PTX/Au NRs in PBS, Medium, and Serum. MUA-PEG/PTX/Au NRs were resuspended in 1× phosphate buffered saline (PBS, pH 7.4, 137 mM NaCl, 2.7 mM KCl, 4.3 mM Na_2HPO_4, and 1.47 mM KH_2PO_4), RPMI 1640 cell culture medium (Mediatech, Inc., Manassas, VA, USA) with 10% fetal bovine serum (FBS) (Gemini Bio-Products, West Sacramento, CA, USA) or 100% FBS to make 1 mL of 0.5 nM (concentration of Au NR) solution. The solution was constantly shaken (600 rpm) on an orbital shaker. At specified times from 30 to 360 min, 200 uL of the solution was withdrawn and centrifuged to separate PTX released from the PTX-Au NR complex. PTX in the supernatant was extracted with an equal volume of DCM, filtered with a 0.22 um syringe filter, and analyzed by UPLC.

PTX Release in a Two-Phase Solution. MUA-PEG/PTX/Au NRs (200 uL, 0.5 nM) in water were added gently on top of 200 uL of DCM solution. At specified times from 10 to 360 min, the organic solution was collected and centrifuged to separate PTX released from the PTX-Au NR complex. After solvent evaporation, the residue was reconstituted with methanol, filtered with 0.22 um syringe filter, and analyzed by UPLC.

PTX Release from MUA-PEG/PTX/Au NRs under Cellular Environment. A549 (lung cancer) cells were seeded at a density of 8×10^3 cells per well into 96-well plates in triplicate. After 24 h, the medium was replaced with 100 uL of fresh medium containing 0.1 nM MUA-PEG/PTX/Au NRs. At a specified time from 30 to 360 min, the cell culture medium was collected. PTX in the medium was extracted with DCM and analyzed with UPLC. PTX released was expressed as the percentage of PTX inside cells compared to the total amount of PTX from the MUA-PEG/PTX/Au NRs added to the medium.

Cell Culture and Cell Viability Assay. KB-3-1 (head and neck cancer) and A549 cells were cultured in RPMI 1640 medium supplemented with 10% (v/v) FBS and pencilium−streptomycin solution (100 U/mL penicillin, 100 U/mL streptomycin) at 37 °C under 5% CO_2. The cells were seeded at a density of 8×10^3 cells per well into 96-well plates in triplicate. After 24 h incubation, PTX (DMSO as the solvent) or equivalent concentration of MUA-PEG/PTX/Au NRs were added at various final concentrations (11, 22, 45, 90, 180, and 360 nM) and were continuously incubated for 24, 48, or 72 h. Cell viability was determined using the XTT ((2,3-bis[2-methoxy-4-nitro-5-sulfophenyl]-2*H*-tetrazolium-5-carboxyanilide inner salt) toxicology assay. The cell viability was expressed as the percentage of live cells over that of the untreated control. The data are presented as the mean ± standard deviation of triplicate measurements. IC_{50} values were determined by fitting the dose−effect curves according to a four-parameter logistic model with *OriginPro 8* software (Origin Lab Corp, Northampton, MA).

dx.doi.org/10.1021/bc300442d | *Bioconjugate Chem.* 2013, 24, 376−386

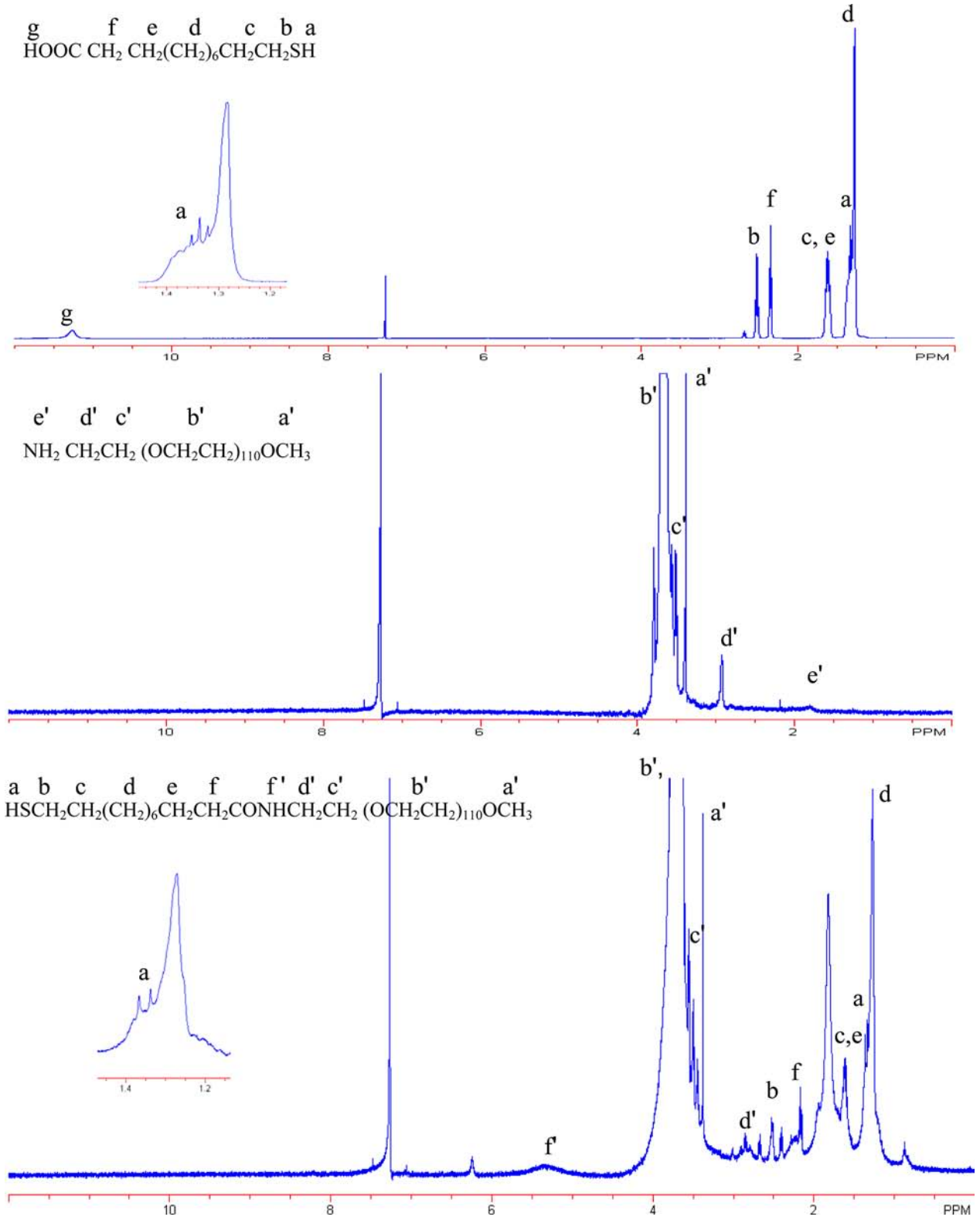

Figure 2. ^{1}H NMR spectra of MUA (top), NH_2-PEG (middle), and MUA-PEG (bottom). The ^{1}H NMR spectrum of MUA-PEG shows a combination of that from MUA and NH_2-PEG, but with the disappearance of the −COOH at 11.25 ppm and appearance of −NH− at 5.35 pm, suggesting the formation of amide bond between MUA and NH_2-PEG. Inset shows the enlarged ^{1}H spectrum of the triplet peak from −SH in MUA.

To examine the potency of combination treatment, the cells were exposed to the following treatments: (1) PTX (DMSO as solvent), (2) MUA-PEG/PTX/Au NRs, (3) MUA-PEG/Au NRs plus laser irradiation, (4) MUA-PEG/PTX/Au NRs plus laser irradiation, and (5) control without any treatment. The laser treatment, 10 min irradiation with NIR light (λ = 808 nm; beam size, 5 mm; power intensity, 0.55 W/cm^2) (Diode laser, Power Technologies, Little Rock, AR) was conducted 2−3 min after addition of drug formulations. Cells were incubated with the drug formulations for 1 h after which they were washed

dx.doi.org/10.1021/bc300442d | *Bioconjugate Chem.* 2013, 24, 376−386

with PBS and incubated in drug-free medium for 48 h. Cell viability was determined using the XTT assay. The concentrations of Au NRs were 0.1, 0.3, and 0.5 nM. Free drug was added at an equivalent concentration of PTX.

Statistical Analysis. Data were expressed as means of three replicated experiments. The statistical significance of the cell viabilities under different treatments, and different concentrations were compared using the analysis of variance (ANOVA). A p-value <0.05 of ANOVA was considered statistically significant in all cases. Multiple comparison procedures were used after obtaining a significant ANOVA result. Hence, a post hoc Scheffe method was applied to determine which means differed. The mean difference between treatments or concentrations was considered to be significant if the absolute value was greater than the minimum significant difference (MSD) which was derived from Scheffe method.

RESULTS AND DISCUSSION

Synthesis and Characterization of Au NRs. In order to maximize photothermal effect in the NIR region, we prepared Au NRs with aspect ratio of 3.7, which were average of 55 nm in length and 15 nm in width (Figure 1A). These Au NRs had a longitudinally localized surface plasmon resonance (LSPR) peak at 780 nm (Figure 1B) which overlapped well with the laser wavelength (785 nm). The surface of the Au NRs have been shown to be capped with the CTAB surfactant in a bilayer structure along the long-axis direction[32] (Scheme 1). In this conformation, one CTAB binds to the Au surface with its ammonium head and interacts with another CTAB with its long hydrocarbon chain. The ammonium headgroup of the second CTAB is exposed to the solution, making the NRs water-soluble and positively charged. The two layers of CTAB provide a hydrophobic pocket that allows direct adsorption of hydrophobic drugs without a need for additional modifications of the drug or the Au NR.

Synthesis and Characterization of MUA-PEG. MUA-PEG was synthesized by the standard DCC-activated coupling reaction in organic phase between PEG-NH_2 and bifunctional MUA. The two molecules were linked by an amide bond leaving the thiol group for binding to Au NRs. We used excessive MUA in order to convert NH_2-PEG to MUA-PEG with high efficiency. The extra MUA after reaction was separated by centrifugal filtration. The formation of MUA-PEG was confirmed by the ^{1}H spectra (Figure 2). MUA gives the characteristic S−H triplet at δ = 1.34 ppm.[33] The strong peak at 1.29 ppm was from the 6 methylene in the alkyl chain. The COOH of MUA gives a weak and broad peak at 11.25 ppm. The NH_2-PEG shows a weak peak at δ = 1.80 ppm from the primary amine.[34] The multiple protons from $-CH_2CH_2O-$ unit give strong peaks from 3.54 to 3.83 ppm. The chemical shift of protons in the $-OCH_3$ group was at 3.38 ppm. The ^{1}H NMR spectrum of MUA-PEG shows a combination of that from MUA and NH_2-PEG, but with the disappearance of the −COOH at 11.25 ppm and the appearance of a weak new peak at 5.35 ppm which was assigned to the secondary amine.[35] These results demonstrated that amide bond was formed between MUA and NH_2-PEG. The lack of a COOH peak indicated that excessive MUA had been successfully separated from the product by centrifugal filtration. Due to the overlap of the signals from primary amine in NH_2-PEG and those from methylene in MUA, it is difficult to determine whether primary amines were present. However, we determined that the ratio of peak area from a and d (−SH and $-(CH_2)_6$) to a′ ($-OCH_3$) is about 4.2, similar to the ratio of these protons in MUA-PEG. This indicates that NH_2-PEG was not present in the product. This is not surprising as we added 2 times more MUA to react with NH_2-PEG in order to completely convert NH_2-PEG to MUA-PEG. The peak at 1.83 ppm was from water that was not completely removed during lyophilization. This was confirmed by the fact that the peak intensity at 1.83 ppm increased when a small amount of water was added to MUA-PEG dissolved in $CDCl_3$ (Figure S1). No other chemicals were found in the product, indicating the high purity of MUA-PEG.

The MUA-PEG was quantified by the absorption spectrum (Figure S2). As shown in Figure S2, MUA-PEG shows an absorption peak at 236 nm, similar to the absorption peak from methoxy-PEG-SH (mPEG-SH, MW 5000, Laysan Bio). We assume mPEG-SH and MUA-PEG have the same absorption coefficient due to their structural similarity. Using the absorption coefficient determined from mPEG-SH (ε = 1.6 × 10^3 M^{-1} cm^{-1}), we determined that the yield of MUA-PEG is 71%. Most likely, sample loss occurred during the multiple periods of centrifugation and washing, which were applied for purification.

Preparation and Characterization of MUA-PEG/PTX/Au NRs. Hydrophobic drugs constitute a large part of commercially available drugs. However, it remains a challenge to load hydrophobic drugs to aqueous NIR-absorbing NPs for PTT-chemotherapy. Previously, You et al. combined PTX with gold nanocages within a poly(lactide-*co*-glycolide) (PLGA) microspheres for light-triggered drug release and PTT-chemotherapy of cancer.[23] In 2009, Kim et al. demonstrated that hydrophobic molecules could be trapped in the Au NP monolayer formed by MUA-linked tetra(ethylene glycol) (TEG) units (MUA-TEG) through a solvent evaporation method.[36] Such a formulation allows drug delivery through hydrophobic interactions of the drug in the nanocomplex with the apolar sites of lipid membrane. For in vivo and clinic applications, a much thicker PEG layer is required to sterically hinder plasma protein adsorption, extend blood circulation time, and correspondingly increase specific tumor accumulation via the EPR effect. Thus, we used MUA-PEG (MW 5000) to entrap PTX on the surface of Au NR.

We made MUA-PEG/PTX/Au NRs via a simple two-step procedure (Scheme 1). First, PTX was adsorbed onto Au NRs via hydrophobic interaction of the molecule with the CTAB capping materials. Then, amphiphilic MUA-PEG was added to replace CTAB while stabilizing the PTX-adsorbed Au NRs. This process was finished within one hour and did not require premodifications of the drug or the carrier. Figure 3 shows the absorption spectra of PTX, Au NRs modified with MUA-PEG only, and Au NRs modified with PTX and MUA-PEG. The absorption spectrum of MUA-PEG/Au NRs is similar to that of CTAB-capped Au NRs (see Figure 1). Although MUA-PEG absorb at 236 nm (Figure S2), MUA-PEG/Au NRs do not show obvious absorption from the surface molecules. This is because the absorption coefficient of MUA-PEG is low, ~10^6 times lower than that of Au NRs. Compared to MUA-PEG modified Au NRs, the MUA-PEG/PTX/Au NRs gave an additional absorption peak at 232 nm from PTX, indicating the success of drug loading. Using UPLC analysis, we found that as much as 2.0 × 10^4 PTX were loaded per Au NR. Using the SPDP method,[31] we determined that 1.1 × 10^4 MUA-PEG were loaded per Au NR. Based on the surface density and the molecular weight of PTX and MUA-PEG as well as the size of Au NR and the density of Au, we determined that the content

dx.doi.org/10.1021/bc300442d | Bioconjugate Chem. 2013, 24, 376−386

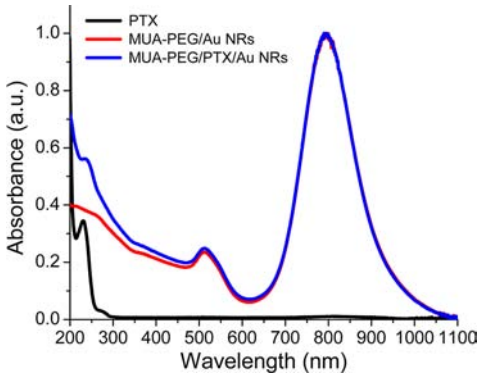

Figure 3. Characterization of PTX loading by absorption spectroscopy. The MUA-PEG/PTX/Au NRs showed the absorption peaks of both PTX and Au NRs, indicating successful formation of PTX-Au NR complexes.

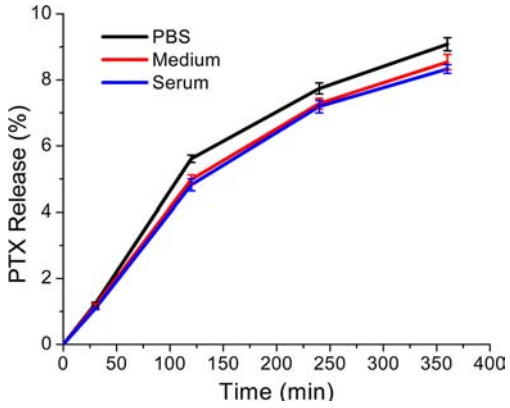

Figure 4. Stability of MUA-PEG/PTX/Au NRs in PBS, cell culture medium, and serum. The solutions were kept constant by shaking on an orbit shaker and the amount of released PTX at different time was measured by UPLC.

of PTX and MUA-PEG in the MUA-PEG/PTX/Au NR was 9.3% (wt %) and 38.7% (wt %), respectively.

DLS measurements (Table 1) showed that CTAB-capped Au NRs had the hydrodynamic size of 49 nm and zeta potential of +37 mV. When the NRs were modified with MUA-PEG alone, the average hydrodynamic size of the NRs increased to 81 nm and the zeta potential decreased to −6 mV. The MUA-PEG/PTX/Au NRs were about 7 nm larger than their MUA-PEG/Au NR in size, but similar in surface charges. These results suggest that MUA-PEG replaced CATB to stabilize the adsorbed PTX rather than displacing the drug from the metal surface. This enabled the formation of highly integrated PTX-Au NR complexes in which PTX is entrapped in the hydrophobic interior of the MUA-PEG monolayer. The hydrophilic PEG exterior makes the nanocomplex physiologically stable.

Table 1. Characterization of Drug Loading by Dynamic Light Scattering

	hydrodynamic size (nm)	zeta potential (mV)
CTAB/Au NRs	48.9 ± 1.3	+37 ± 1.8
MUA-PEG/Au NRs	81.3 ± 2.1	−5.8 ± 0.3
MUA-PEG/PTX/Au NRs	87.9 ± 1.8	−7.4 ± 0.6

Stability of MUA-PEG/PTX/Au NRs in PBS, Medium, and Serum. One of the key issues for successful combination treatment is controlling the drug release at tumor sites. The nanocomplex should not exhibit significant drug release in the off-target blood system. We therefore examined whether the nanocomplexes were stable in PBS, cell culture medium, and 100% serum under mobile conditions. To mimic blood circulation, the nanocomplxes in the above solutions were continuously shaken on an orbit shaker. An aliquot of the solution was extracted at different times, processed with solvent extraction, and analyzed with UPLC to determine the content of released PTX. We found that only 1% of PTX was released after 1 h in all the solutions (Figure 4). After 6 h, less than 10% of PTX was released in all cases. These results demonstrate that the nanocomplexes are stable in PBS, medium, or serum, indicating their great stability in blood circulation.

PTX Release from MUA-PEG/PTX/Au NRs in a Two-Phase Solution and in Cellular Environment. Hydrophobic drugs preferentially localize to apolar sites, such as lipid membranes, with a high partition coefficient.[37] This property provides a great opportunity for intracellular delivery of hydrophobic drugs without the use of external triggers.[36,38] To demonstrate PTX release from the MUA-PEG/PTX/Au NRs in vitro, we used a water/DCM two-phase solution to mimic the lipid membrane. In this study, MUA-PEG/PTX/Au NRs were exposed to an equal volume of DCM and the amount of PTX in the organic phase was quantified as a function of time by UPLC. The nanocomplex exhibited a biphasic release profile with the rapid release process occurring within 2 h (Figure 5A). At this time, 50% PTX was released from the complex. At 6 h, the amount of released PTX increased to 76%, suggesting highly efficient drug release of the nanocomplex. The drug release process occurred at the water−DCM interface, based on the fact that only a trace amount of Au NRs (<5%) was found in the organic phase. A potential concern with the two-phase model is the dissociation of MUA-PEG from the surface of Au NR due to the solvent extraction, which could accelerate the release of PTX. To examine whether MUA-PEG was displaced from the surface of Au NR during extraction, we measured the ^{1}H spectrum of the organic phase at 3 h after mixing 200 uL of 0.5 nM MUA-PEG/Au NRs and 200 uL of DCM. Figure S3 shows that no chemicals were found in the DCM phase. This indicates that MUA-PEG was not displaced during the two-phase studies.

We have demonstrated efficient PTX release using a membrane-mimic water/DCM system. However, the two-phase system does not represent a true model of a cell system. Thus, we further examined the drug release profile when the nanocomplexes were exposed to cancer cells. In this study, we incubated A549 cells with cell culture medium containing MUA-PEG/PTX/Au NRs. After a specified time from 10 to 360 min, we determined the amount of PTX inside cancer cells by measuring PTX remaining in the supernatant medium at different incubation times. Figure 5B shows the percentage of PTX released (i.e., percentage of PTX inside cells) when MUA-PEG/PTX/Au NRs (0.1 nM, 100 uL) were incubated with A549 cells (in 96-well plate). The nanocomplex exhibited a biphasic release profile with the rapid release process occurring within the first hour. Then, PTX release was slowly increased, with 64% of PTX released at 6 h. PTX release in the presence of cells is significantly accelerated compared to that in the absence of cells (Figure 4). This could be due to the effects from increased temperature (room temperature to 37 °C) and the presence of cells. To examine the temperature effects, we

dx.doi.org/10.1021/bc300442d | Bioconjugate Chem. 2013, 24, 376−386

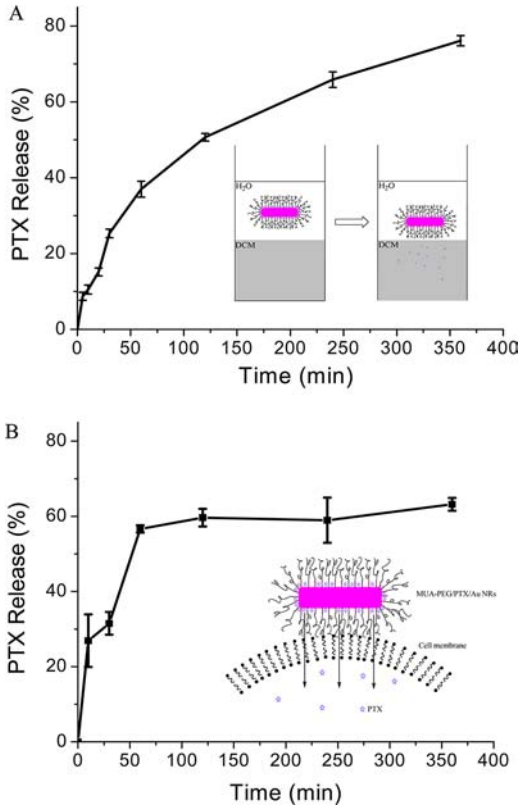

Figure 5. (A) Release profile of PTX from MUA-PEG/PTX/Au NRs in a two-phase solution. 200 uL of 0.5 nM MUA-PEG-PTX/Au NRs in water was exposed to equal amount of DCM. PTX in the DCM layer at different time was quantified with UPLC. (B) Release profile of PTX from MUA-PEG/PTX/Au NRs under cellular environment. A549 cells (in 96-well cell culture plate) were exposed to 100 μL of cell culture medium containing 0.1 nM MUA-PEG-PTX/Au NRs. PTX in cells was quantified by determination of PTX in the supernatant of medium with UPLC.

incubated cell culture medium containing MUA-PEG/PTX/Au NRs at 37 °C for 6 h and then measured free PTX in the medium. We found that 13% PTX was released, which was slightly higher than that at room temperature (9%). Thus, the high efficiency of drug release in the presence of cells was mainly due to the effects from the lipid membrane of cells.

Cytotoxicity of MUA-PEG/PTX/Au NRs. Chemotherapy is one of the major components in the combination treatment. Therefore, we first determined the anticancer activity of MUA-PEG/PTX/Au NRs as a chemotherapeutic agent using XTT assay. Two cell lines with different origins: KB-3-1 head and neck cancer and A549 lung cancer were used to test our reagents. Figure 6 shows the percentage viabilities of KB-3-1 and A549 cells (relative to the control) after 24, 48, and 72 h incubation with free PTX delivered in DMSO and MUA-PEG/PTX/Au NRs at varying PTX concentrations. Both free PTX and PTX-loaded Au NRs showed time- and dose-dependent anticancer activities. The nanocomplex showed comparable cytotoxicity to the free drug against both cell lines. Table 2 summarizes the IC_{50} of free PTX and MUA-PEG/PTX/Au NRs under different conditions. The IC_{50} of MUA-PEG/PTX/Au NRs ranged from 20 to 100 nM depending on the incubation time and the cell line. Increasing the drug exposure time leads to decreased IC_{50} and thus a better cell killing effect of the drug. The MUA-PEG/PTX/Au NRs showed slightly higher IC_{50} than free PTX in KB-3-1 cells, but vice versa in A549 cells. The delayed drug release from the nanocomplex generally leads to lower cell killing potency of the nanocomplex than the free drug. However, the sustained drug release may protect PTX from epimerization and hydrolysis in the cellular environment and thus lead to higher cytotoxicity for the nanocomplx. These factors could lead to the difference between the two cell lines in the anticancer activity of the nanodrug relative to the free drug.

Cytotoxicity of MUA-PEG/PTX/Au NRs Combined with Laser Irradiation. To examine the capabilities of the nanocomplexes for combined PTT and chemotherapy, we compared the cytotoxic effects of PTX delivered in DMSO (chemotherapy without the use of carriers), MUA-PEG/PTX/Au NRs without laser irradiation (chemotherapy using Au NR carriers), MUA-PEG/PTX/Au NRs with laser irradiation (combined PTT and chemotherapy), and MUA-PEG/Au NRs plus laser irradiation (PTT) in both KB and A549 cells. Free PTX is shown to have blood half-life around 1 h.[39] Thus, in these studies, cells were exposed to drugs for 1 h with or without laser irradiation. Then, the cells were washed three times with PBS to remove drugs and incubated in drug-free medium for 48 h followed by XTT assay. Figure 7 shows the cell viabilities under different treatments at three dosages. Statistical analysis with ANOVA followed by pairwise comparisons using the Scheffe method showed significant differences ($P < 0.05$, mean difference > MSD) between the combination treatment and PTT, chemotherapy with MUA-PEG/PTX/Au NRs, or chemotherapy with free PTX (Table S1−6). These differences were reproducible in both cell lines and at multiple dosages. For example, KB-3-1 cells treated with 0.1 nM MUA-PEG/PTX/Au NRs and 0.1 nM MUA-PEG/Au NRs plus laser irradiation showed cell viabilities of 36.5% and 45.1%, respectively. However, when these cells were treated with 0.1 nM MUA-PEG/PTX/Au NRs plus laser irradiation (the combination therapy), cell viability decreased markedly to 6.8%. This combination treatment killed about 30% more cells than the chemotherapy and about 40% more cells than the PTT. Similar findings were observed with A549 cells. The MUA-PEG/PTX/Au NRs showed lower cytotoxicity than the free PTX in chemotherapy. This is not surprising, as it takes time for the nanocomplex to completely release the loaded drugs.

Increasing the concentration of the drug formulations led to increased cell killing effects for all treated groups. In the KB-3-1 cell model, viabilities under the chemotherapy with free PTX, chemotherapy with MUA-PEG/PTX/Au NRs, and PTT with MUA-PEG/Au NRs decreased to 6.2%, 17.6%, and 13.2% at 0.5 nM nanocomplex and equivalent PTX. No live cells were detected under the combination treatment. Similarly, cells were completely eradicated under combination treatment for A549 cells while all other treatment groups showed higher than 5% viabilities. At the 0.5 nM Au NR dosage, the temperature of the medium with respective to the laser-treated groups was increased to 58 °C. This temperature has been previously demonstrated to induce maximal photothermal tumor killing without inducing severe tissue bleach and burning in vivo.[7] The 0.1 and 0.3 nM Au NRs raised the temperature of the medium to 43 and 51 °C, respectively.

Thermal effect of cells could increase membrane permeability, and thus increasing drug diffusion. It could also change the drug uptake kinetics. These factors may lead to a synergistic effect between the PTT and chemotherapy, amplifying the

dx.doi.org/10.1021/bc300442d | Bioconjugate Chem. 2013, 24, 376−386

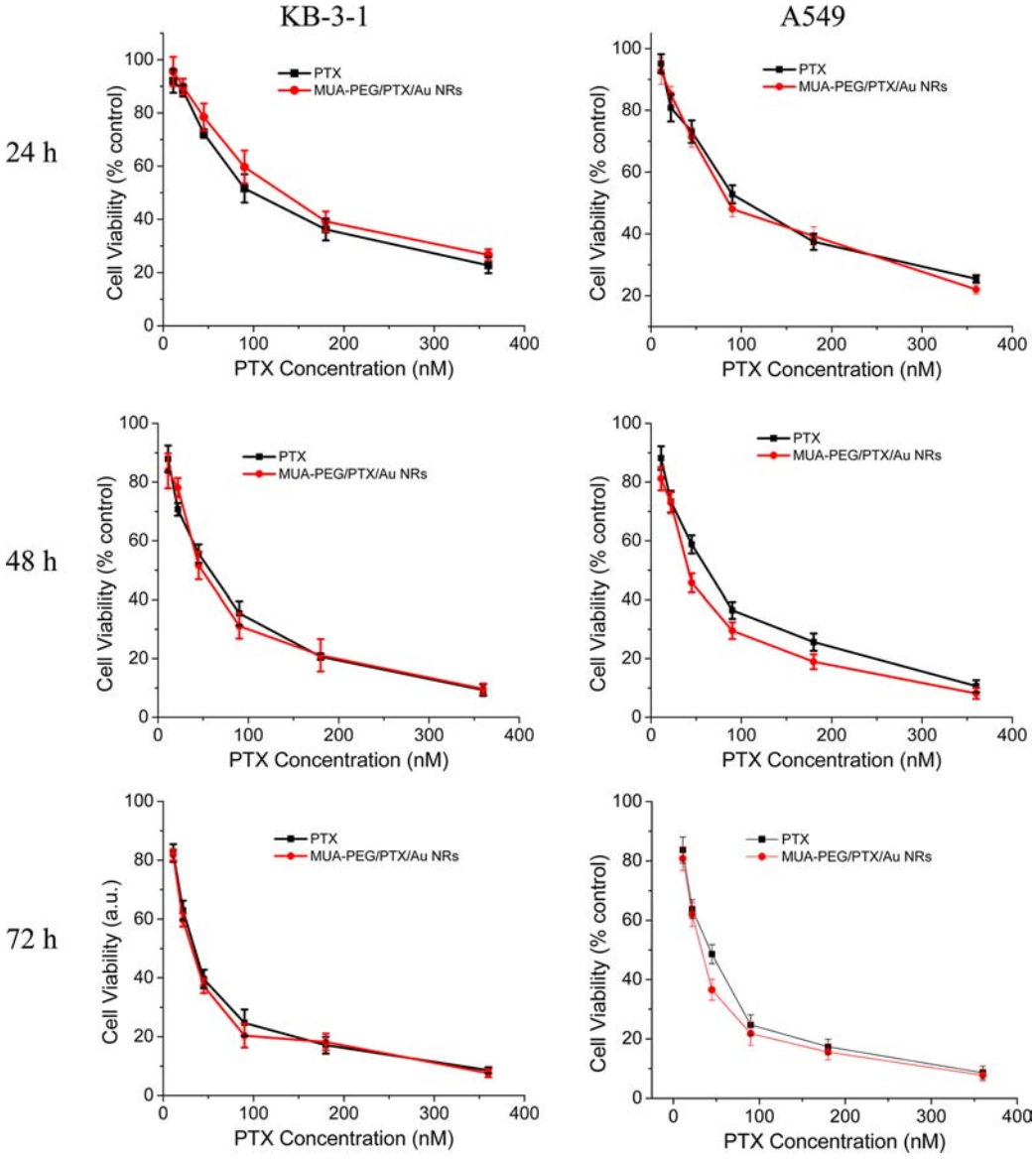

Figure 6. Cytotoxicity of free PTX and MUA-PEG/PTX/Au NRs in KB-3-1 and A549 cells after 24, 48, and 72 h incubation. The results are mean values ± SD of triplicate experiments. The MUA-PEG/PTX/Au NRs showed comparable anticancer activity to the free PTX in both cell lines. The concentration of MUA-PEG/PTX/Au NRs was expressed as equivalent PTX concentration.

Table 2. IC_{50} of Free PTX and MUA-PEG/PTX/Au NRs after 24, 48, and 72 h Incubation in KB-3-1 and A549 Cells

		IC_{50} (nM PTX)	
cell line	incubation time (h)	PTX	MUA-PEG/PTX/Au NRs
KB-3-1	24	80 ± 2.0	96 ± 2.4
	48	45 ± 0.8	50 ± 1.1
	72	22 ± 0.1	24 ± 0.4
A549	24	83 ± 2.5	77 ± 1.6
	48	53 ± 1.2	44 ± 1.7
	72	31 ± 0.5	23 ± 0.3

therapeutic outcome dramatically. To determine whether a synergist effect exists in the combination treatment in our system, cell viability was compared to the calculated value from the additive effect. The additive cell viability was calculated according to the following relationship[16]

$$f_{\text{additive}} = f_{\text{PTT}} \times f_{\text{chemotherapy}} \quad (1)$$

where f_{additive} is the fraction of surviving cells by additive interaction of PTT and chemotherapy, f_{PTT} is the fraction of surviving cells resulting from PTT treatment, and $f_{\text{chemotherapy}}$ is the fraction of surviving cells resulting from chemotherapy. When the fraction of surviving cells from the combination treatment, $f_{\text{combination}}$, is lower than f_{additive}, there is a synergistic effect. When $f_{\text{combination}} = f_{\text{additive}}$, it is an additive effect. The calculated f_{additive} for both cell lines is listed in Table 3. The experimental $f_{\text{combination}}$ values of MUA/PTX/Au NRs are lower than the calculated f_{additive} values in both KB and A549 cells, regardless of the concentration of the nanocomplexes. To further examine whether a synergistic effect exists, we compared the cellular uptake of PTX with and without laser irradiation using A549 cells. Figure S4 shows the percentage of PTX inside A549 cells (1 h incubation) when the cells were exposed to 0.1 nM MUA-PEG/PTX/Au NRs, with and without laser irradiation. Laser irradiation increased cellular uptake of PTX by ~10%, which is significantly different from those without laser irradiation (P = 0.006). Thus, a synergistic effect existed

dx.doi.org/10.1021/bc300442d | Bioconjugate Chem. 2013, 24, 376−386

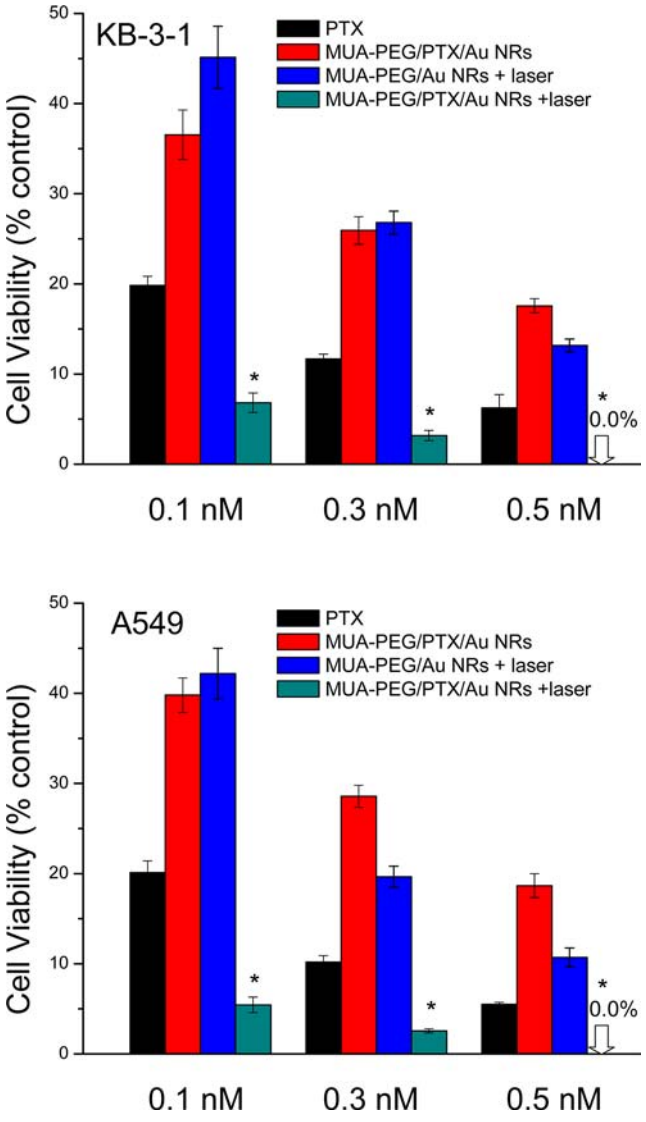

Figure 7. Cytotoxicity of PTX, MUA-PEG/Au NRs with laser irradiation, and MUA-PEG/PTX/Au NRs with and without laser irradiation in KB-3-1 and A549 cells. Cells were incubated with PTX-equivalent drug formulations for one hour with or without laser irradiation, followed by incubation in drug-free medium for 48 h before XTT assay. Laser irradiation was performed by exposing the cells to NIR light (λ = 808 nm) for 10 min at the power density of 0.55 W/cm^2. The results are mean values ± SD of triplicate experiments. Combined PTT and chemotherapy with MUA-PEG/PTX/Au NRs showed excellent anticancer activity, superior to PTT or chemotherapy alone at all drug dosages. (*P < 0.05 and mean difference > MSD compared with free PTX, MUA-PEG/PTX/Au NRs, and MUA-PEG/Au NRs plus laser irradiation). Drug concentration was expressed as equivalent concentration of Au NRs.

between PTT and chemotherapy using the MUA-PEG/PTX/Au NRs for combination cancer therapy.

CONCLUSIONS

We have developed a new single particle drug delivery system for PTT-chemotherapy of cancer. Hydrophobic PTX was successfully loaded onto NIR-absorbing Au NRs with high density (2.0 × 10^4 PTX/Au NR) via a simple, fast, and highly efficient method without premodifications of the drug and the carrier. The compact nanocomplexes were stable in cell-absent environments conditions, but efficiently released their drug payload to exert cytotoxic effects via hydrophobic interactions of the drug and the apolar lipid membrane. Combined PTT and chemotherapy using the MUA-PEG/PTX/Au NRs was demonstrated to be synergistic and highly effective, leading to complete eradication of cultured cancer cells in vitro at a dosage of 0.5 nM nanocomplex with low intensity (0.55 W/cm^2) NIR light. We expect the novel nanocomplex to be able to deliver high concentration of PTX to tumor sites to eradicate malignant cells synergistically with PTT. The resulting platform may prevent tumor regrowth and metastasis and have important impact on the treatment of head and neck cancer and other malignancies in the clinic.

Table 3. Calculated Fraction of Cell Survival by Additive Interaction of PTT and Chemotherapy Using MUA-PEG/PTX/Au NR

cell line	MUA-PEG/PTX/Au NR concentration (nM)	additive cell viability (% control)
KB-3-1	0.1	16.4
	0.3	6.9
	0.5	2.3
A549	0.1	16.8
	0.3	5.6
	0.5	2.0

ASSOCIATED CONTENT

Supporting Information

Results of the statistical analysis on the cytotoxicity of MUA-PEG/PTX/Au NRs combined with laser irradiation, ^{1}H NMR spectrum of MUA-PEG in the presence of water, absorption spectrum of MUA-PEG and mPEG-SH, ^{1}H NMR spectra of the DCM phase after mixing MUA-PEG/Au NRs aqueous solution with DCM and cellular uptake of PTX from MUA-PEG/PTX/Au NRs with and without laser irradiation. This material is available free of charge via the Internet at http://pubs.acs.org.

AUTHOR INFORMATION

Corresponding Author

*E-mail: xhuang4@memphis.edu. Tel: (901) 678 1728. Fax: (901) 678 3744.

Present Address

[#]Department of Pharmacy, Nanfan Hospital, Southern Medical University, Guangzhou, 510515, PR China.

Author Contributions

[Δ]F. R and S. B. contributed equally.

Notes

The authors declare no competing financial interest.

ACKNOWLEDGMENTS

Huang acknowledges financial supported by the University of Memphis Faculty Research grant. We also thank Bing Yan, Kip Guy, Hongyu Zhou, and Cynthia Jeffries at St. Jude Children Research Hospital for UPLC analysis.

REFERENCES

(1) Hirsch, L. R., Stafford, R. J., Bankson, J. A., Sershen, S. R., Price, R. E., Hazle, J. D., Halas, N. J., and West, J. L. (2003) Nanoshell-mediated near infrared thermal therapy of tumors under MR guidance. *Proc. Natl. Acad. Sci. U.S.A. 100*, 13549−13554.

(2) O'Neal, D. P., Hirsch, L. R., Halas, N. J., Payne, J. D., and West, J. L. (2004) Photothermal tumor ablation in mice using near infrared absorbing nanoshells. *Cancer Lett. 209*, 171−176.
(3) Loo, C., Hirsch, L., Lee, M. H., Chang, E., West, J., Halas, N., and Drezek, R. (2005) Gold nanoshell bioconjugates for molecular imaging in living cells. *Opt. Lett. 30*, 1012−1014.
(4) Loo, C., Lowery, A., Halas, N. J., West, J. L., and Drezek, R. (2005) Immunotargeted nanoshells for integrated cancer imaging and therapy. *Nano Lett. 5*, 709−711.
(5) Lal, S., Clare, S. E., and Halas, N. J. (2008) Nanoshell-enabled photothermal cancer therapy: impending clinical impact. *Acc. Chem. Res. 41*, 1842−1851.
(6) Huang, X., El-Sayed, I. H., Qian, W., and El-Sayed, M. A. (2006) Cancer cell imaging and photothermal therapy in the near-infrared region by using gold nanorods. *J. Am. Chem. Soc. 128*, 2115−2120.
(7) Dickerson, E. B., Dreaden, E. C., Huang, X., El-Sayed, I. H., Chu, H., Pushpanketh, S., McDonald, J. F., and El-Sayed, M. A. (2008) Gold nanorod assisted near-infrared plasmonic photothermal therapy (PPTT) of squamous cell carcinoma in mice. *Cancer Lett. 269*, 57−66.
(8) Huang, X., Neretina, S., and El-Sayed, M. A. (2009) Gold nanorods: from synthesis and properties to biological and biomedical applications. *Adv. Mater. 21*, 4880−4910.
(9) Tong, L., Zhao, Y., Huff, T. B., Hansen, M. N., Wei, A., and Cheng, J. X. (2007) Gold nanorods mediate tumor cell death by compromising membrane integrity. *Adv. Mater. 19*, 3136−3141.
(10) von Maltzahn, G., Park, J. H., Agrawal, A., Bandaru, N. K., Das, S. K., Sailor, M. J., and Bhatia, S. N. (2009) Computationally guided photothermal tumor therapy using long-circulating gold nanorod antennas. *Cancer Res. 69*, 3892−3900.
(11) Chen, J., Wang, D., Xi, J., Au, L., Siekkinen, A., Warsen, A., Li, Z. Y., Zhang, H., Xia, Y., and Li, X. (2007) Immuno gold nanocages with tailored optical properties for targeted photothermal destruction of cancer cells. *Nano Lett. 7*, 1318−1322.
(12) Chen, J., Glaus, C., Laforest, R., Zhang, Q., Yang, M., Gidding, M., Welch, M. J., and Xia, Y. (2010) Gold nanocages as photothermal transducers for cancer treatment. *Small 6*, 811−817.
(13) Melancon, M. P., Lu, W., Yang, Z., Zhang, R., Cheng, Z., Elliot, A. M., Stafford, J., Olson, T., Zhang, J. Z., and Li, C. (2008) In vitro and in vivo targeting of hollow gold nanoshells directed at epidermal growth factor receptor for photothermal ablation therapy. *Mol. Cancer Ther. 7*, 1730−1739.
(14) Lu, W., Xiong, C., Zhang, G., Huang, Q., Zhang, R., Zhang, J. Z., and Li, C. (2009) Targeted photothermal ablation of murine melanomas with melanocyte-stimulating hormone analog conjugated hollow gold nanospheres. *Clin. Cancer Res. 15*, 876−886.
(15) Kam, N. W. S., O'Connell, M., Wisdom, J. A., and Dai, H. (2005) Carbon nanotubes as multifunctional biological transporters and near-infrared agents for selective cancer cell destruction. *Proc. Natl. Acad. Sci. U.S.A. 102*, 11600−11605.
(16) Hauck, T. S., Jennings, T. L., Yatsenko, T., Kumaradas, J. C., and Chan, W. C. W. (2008) Enhancing the toxicity of cancer chemotherapeutics with gold nanorod hyperthermia. *Adv. Mater. 20*, 3832−3838.
(17) Park, H., Yang, J., Lee, J., Haam, S., Choi, I. H., and Yoo, K. H. (2009) Multifunctional nanoparticles for combined doxorubicin and photothermal treatments. *ACS Nano 3*, 2919−2926.
(18) You, J., Zhang, G., and Li, C. (2010) Exceptionally high payload of doxorubicin in hollow gold nanospheres for near-infrared light-triggered drug release. *ACS Nano 4*, 1033−1041.
(19) You, J., Zhang, R., Zhang, G., Zhong, M., Liu, Y., Van Pelt, C. S., Liang, D., Wei, W., Sood, A. K., and Li, C. (2012) Photothermal-chemotherapy with doxorubicin-loaded hollow gold nanospheres: A platform for near-infrared light-trigged drug release. *J. Controlled Release 158*, 319−328.
(20) Liu, H., Chen, D., Li, L., Liu, T., Tan, L., Wu, X., and Tang, F. (2011) Multifunctional gold nanoshells on silica nanorattles: a platform for the combination of photothermal therapy and chemotherapy with low systemic toxicity. *Angew. Chem., Int. Ed. 50*, 891−895.
(21) Hribar, K. C., Lee, M. H., Lee, D., and Burdick, J. A. (2011) Enhanced release of small molecules from near-infrared light responsive polymer-nanorod composites. *ACS Nano 5*, 2948−2956.
(22) Cheng, F. Y., Su, C. H., Wu, P. C., and Yeh, C. S. (2010) Multifunctional polymeric nanoparticles for combined chemotherapeutic and near-infrared photothermal cancer therapy in vitro and in vivo. *Chem. Commun. 46*, 3167−3169.
(23) You, J., Shao, R., Wei, X., Gupta, S., and Li, C. (2010) Near-infrared light triggers release of paclitaxel from biodegradable microspheres: photothermal effect and enhanced antitumor activity. *Small 6*, 1022−1031.
(24) Kuo, T. R., Hovhannisyan, V. A., Chao, Y. C., Chao, S. L., Chiang, S. J., Lin, S. J., Dong, C. Y., and Chen, C. C. (2010) Multiple release kinetics of targeted drug from gold nanorod embedded polyelectrolyte conjugates induced by near-infrared laser irradiation. *J. Am. Chem. Soc. 132*, 14163−14171.
(25) Wu, W., Shen, J., Banerjee, P., and Zhou, S. (2011) Water-dispersible multifunctional hybrid nanogels for combined curcumin and photothermal therapy. *Biomaterials 32*, 598−609.
(26) van Vlerken, L. E., Vyas, T. K., and Amiji, M. M. (2007) Poly(ethylene glycol)-modified nanocarriers for tumor-targeted and intracellular delivery. *Pharm. Res. 24*, 1405−1414.
(27) Fang, J., Nakamura, H., and Maeda, H. (2011) The EPR effect: Unique features of tumor blood vessels for drug delivery, factors involved, and limitations and augmentation of the effect. *Adv. Drug Delivery Rev. 63*, 136−151.
(28) Nikoobakht, B., and El-Sayed, M. A. (2003) Preparation and growth mechanism of gold nanorods (NRs) using seed-mediated growth method. *Chem. Mater. 15*, 1957−1961.
(29) Orendorff, C. J., and Murphy, C. J. (2006) Quantitation of metal content in the silver-assisted growth of gold nanorods. *J. Phys. Chem. B 110*, 3990−3994.
(30) Huang, X., Peng, X., Wang, Y., Wang, X., Shin, D. M., El-Sayed, M. A., and Nie, S. (2010) A reexamination of active and passive tumor targeting by using rod-shaped gold nanocrystals and covalently conjugated peptide ligands. *ACS Nano 4*, 5887−5896.
(31) Josephson, L., Tung, C. H., Moore, A., and Weissleder, R. (1999) High-efficiency intracellular magnetic labeling with novel superparamagnetic-tat peptide conjugates. *Bioconjugate Chem. 10*, 186−191.
(32) Nikoobakht, B., and El-Sayed, M. A. (2001) Evidence for bilayer assembly of cationic surfactants on the surface of gold nanorods. *Langmuir 17*, 6368−6374.
(33) Su, C. H., Wu, P. L., and Yeh, C. S. (2004) pH dependence of interparticle coupling for gold nanoparticle assemblies formation: electrostatic attraction and hydrogen bonding. *Bull. Chem. Soc. Jpn. 77*, 189−193.
(34) Liu, R., He, B., Li, D., Lai, Y., Chang, J., Tang, J. Z., and Gu, Z. (2012) Effects of pH-sensitive chain length on release of doxorubicin from mPEG-b-PH-b-PLLA nanoparticles. *Int. J. Nanomed. 7*, 4433−4446.
(35) Upadhyayula, S., Bao, D., Millare, B., Sylvia, S. S., Habib, K. M. M., Ashraf, K., Ferreira, A., Bishop, S., Bonderer, R., Baqai, S., Jing, X., Penchev, M., Ozkan, M., Ozkan, C. S., Lake, R. K., and Vullev, V. I. (2011) Permanent electric dipole moments of carboxyamides in condensed media: what are the limitations of theory and experiment? *J. Phys. Chem. B 115*, 9473−9490.
(36) Kim, C. K., Ghosh, P., Pagliuca, C., Zhu, Z. J., Menichetti, S., and Rotello, V. M. (2009) Entrapment of hydrophobic drugs in nanoparticle monolayers with efficient release into cancer cells. *J. Am. Chem. Soc. 131*, 1360−1361.
(37) Wenk, M. R., Fahr, A., Reszka, R., and Seelig, J. (1996) Paclitaxel partitioning into lipid bilayers. *J. Pharm. Sci. 85*, 228−231.
(38) Cheng, Y., Samia, A. C., Meyers, J. D., Panagopoulos, I., Fei, B., and Burda, C. (2008) Highly efficient drug delivery with gold nanoparticle vectors for in vivo photodynamic therapy of cancer. *J. Am. Chem. Soc. 130*, 10643−10647.
(39) Eiseman, J. L., Eddington, N. D., Leslie, J., MacAuley, C., Sentz, D. L., Zuhowski, M., Kujawa, J. M., Yong, D., and Egorin, M. J. (1994)

Plasma pharmacokinetics and tissue distribution of paclitaxel in CD2F1 mice. *Cancer Chemother. Pharmacol. 34*, 465−471.